Validation Study of the CAPS Model Land Surface Scheme Using the 1987 Cabauw/PILPS Dataset

S. CHANG,* D. HAHN, C.-H. YANG, AND D. NORQUIST

Phillips Laboratory, Geophysics Directorate, Hanscom Air Force Base, Massachusetts

M. EK

Oceanic and Atmospheric Sciences, Oregon State University, Corvallis, Oregon

(Manuscript received 15 September 1997, in final form 11 May 1998)

ABSTRACT

An updated complete and comprehensive description of the land surface parameterization scheme in the Coupled Atmosphere–Plant–Soil (CAPS) model is presented. The CAPS model has been in development at Oregon State University and Phillips Laboratory since 1981. The CAPS model was originally designed for a global atmospheric model, but it has also been used as a stand-alone model for a variety of applications. The land surface scheme in the CAPS model is one of the two dozen schemes that participated in the Project for Intercomparison of Land Surface Parameterization Schemes (PILPS). Some unique features of the CAPS scheme are given in detail. A comprehensive dataset of one year (1987), including atmospheric forcing data and validation data from Cabauw, has been provided for PILPS by the Royal Netherlands Meteorological Institute. Using the Cabauw data, a validation study for the CAPS scheme has been carried out. The scheme's self-consistencies in terms of surface energy balance and water budget are discussed. Finally, the results of this validation study with emphasis on the performance of surface momentum and heat fluxes are presented.

1. Introduction

Mahrt and Ek (1984), Mahrt and Pan (1984), Troen and Mahrt (1986), Ek and Mahrt (1991a) at Oregon State University (OSU) have developed a coupled atmospheric boundary layer (ABL) and soil–vegetation model for the Phillips Laboratory (PL, formerly the Air Force Geophysics Laboratory) Global Spectral Model (GSM) for numerical weather prediction. Norquist and Chang (1994) provided a brief description of the PL GSM physics, including the OSU model physics. In addition, the OSU One-Dimensional (1D) ABL Model User's Guide by Ek and Mahrt (1991b), with contributions by many people, has documented the evolved algorithm and code of the model. During the past decade, the OSU 1D model has been adapted, tested, and improved continuously within the PL GSM. The OSU model has also been formulated for inclusion in other large-scale models (e.g., Pan 1990). The model has also been used as a stand-alone model for a number of numerical experiments under various geophysical conditions (e.g., Xinmei and Lyons 1995; Kim and Ek 1995; Chen et al. 1996). The model and its code were requested and used by two dozen research groups worldwide (about 10 countries) for a variety of applications. Interactions with many model users provide us with numerous comments that enhance our ability to make continuous corrections and improvements.

Although the model has been used and tested for a decade, it still needs comprehensive validation and evaluation, especially the soil–vegetation part of the model. Recently, the Project for Intercomparison of Land Surface Parameterization Schemes (PILPS) provided an excellent opportunity to test and compare many different land surface parameterization schemes using various numerical and observational datasets (Henderson-Sellers et al. 1993; Henderson-Sellers et al. 1995). The original OSU model consists of two major components: 1) the atmospheric boundary layer including the surface layer model and 2) the two-layer soil and simple plant model (Pan and Mahrt 1987). The bulk of the OSU model, namely, the surface layer part and the two-layer soil–vegetation part, has been reorganized into a single scheme for participation in PILPS. In PILPS, this scheme is known as the Coupled Atmosphere Boundary Layer–Plant–Soil (CAPS) model land surface parameterization scheme, or ''the CAPS scheme'' for brevity. Starting in 1992, the ongoing PILPS study has produced

* Current affiliation: Army Research Laboratory, Adelphi, Maryland.

Corresponding author address: Dr. Sam S. Chang, BLDG 202 4F076, Army Research Laboratory, 2800 Powder Mill Rd., ATTN AMSRL IS EM (DR. CHANG), Adelphi, MD 20783-1197.
E-mail: chang@plh.af.mil

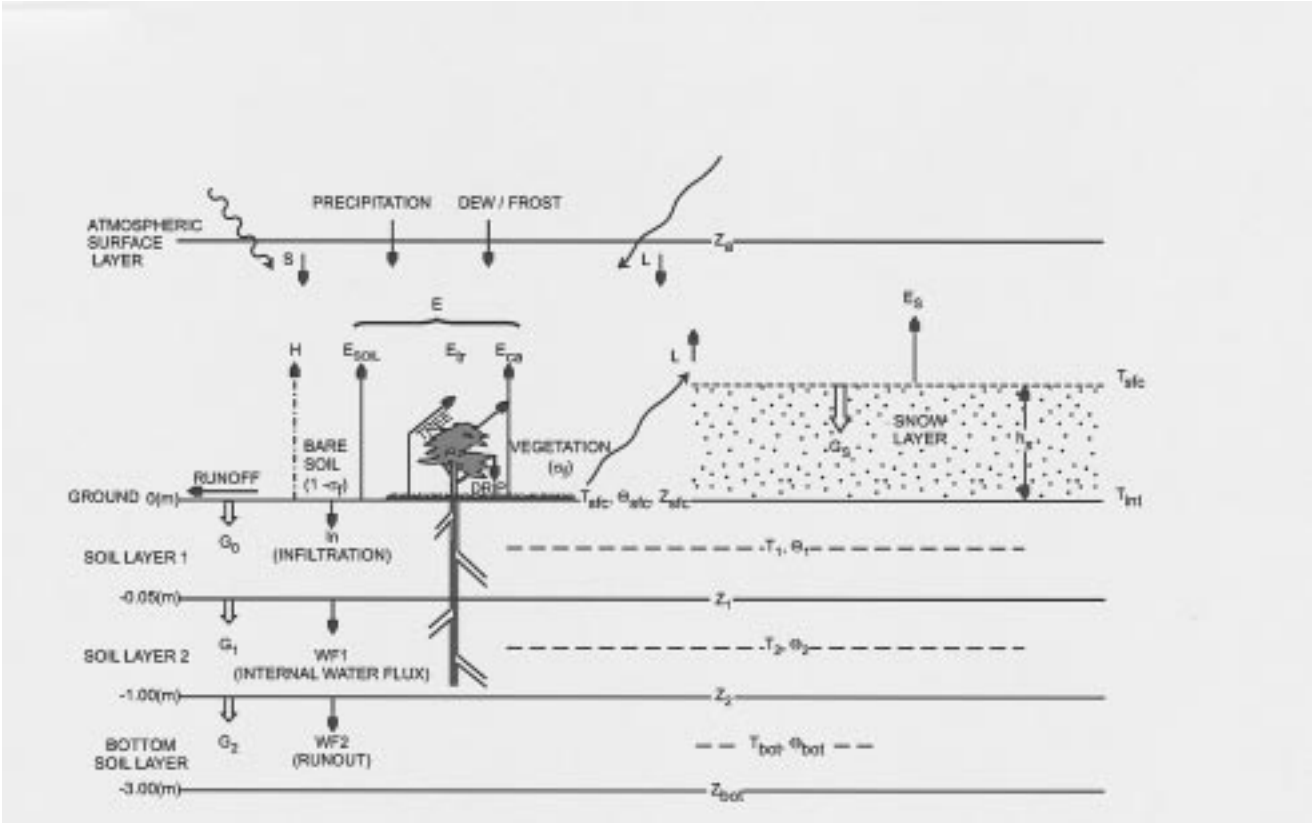

FIG. 1. A schematic of the geometry of the CAPS land surface parameterization scheme is shown. The left side illustrates the situation of no snow cover on the ground surface. The term σ_f denotes the fraction of the surface covered by vegetation. Arrows indicate fluxes: $S\downarrow$, $L\downarrow$, and $L\uparrow$ are the downward solar shortwave radiation, the downward atmospheric longwave radiation, and the upward terrestrial longwave radiation, respectively. The total evapotranspiration (E) includes E_{soil} (evaporation from the bare soil), E_{tr} (transpiration from the vegetation), and E_{ca} (direct evaporation of the canopy water). Here H is the sensible heat flux. The open arrows (G_0, G_1, and G_2) represent the soil heat fluxes. Two dashed lines indicate the middle level of each soil layer, which is the location of computation of the soil temperature (T) and soil water content (Θ). The subscripts (sfc, 1, 2, and bot) refer to the surface, first, second, and bottom soil layers. The water fluxes in the soil are denoted by In, WF1, and WF2. The reference height in the atmospheric surface layer is denoted by Z_a. The right side illustrates the situation of snow cover. Here h_s is the snow cover depth, G_s is the heat flux within the snow layer, and T_{sfc} and T_{int} represents the temperature at snow surface and at the interface between the snow layer and the first soil layer.

important results and recommendations from PILPS phase 1 (Pitman et al. 1993) and PILPS phase 2 (Chen et al. 1997). Better documentation and systematic sensitivity tests of each of those participating schemes in PILPS has been highly recommended. The PILPS has provided not only important intercomparison results of two dozen land surface parameterization schemes but also a valuable data bank. In particular, PILPS phase 2a has provided a 1-yr dataset of both atmospheric forcing and surface fluxes observed from Cabauw, the Netherlands. The valuable Cabauw dataset has allowed the CAPS scheme to be tested in a series of zero-dimensional (offline) numerical experiments. The results of those experiments can help us to obtain new insights into the scheme's performance, validity, and sensitivity; to identify the weakest parts of the scheme; and to dictate the future direction of the research on the scheme's improvements. Chang and Ek (1996) have recently reported the results of the CAPS scheme's sensitivity experiments.

The objectives of this paper are twofold. The first objective is to provide an updated, concise description of the CAPS scheme as systematically and completely as possible (section 2) for the following reasons. Despite the fact that a number of papers and documents on the CAPS scheme have been published, the existing papers and documents for the scheme are found in many different sources over a period of more than a decade, many of the previous papers contain a number of old parameterizations, and many modifications and improvements in the CAPS scheme contained in the current code have not been formally described. For example, the snow package and the water balance formulation have not been clearly and rigorously documented. The second objective is to present the results of the numerical experiments for the scheme's performance using the

Cabauw dataset. Section 3 describes our numerical experiments, the results of which are discussed in section 4. The last section gives a summary and conclusions from the current study of the CAPS scheme.

2. Description of the model

a. Geometry

The current standard version of the 1D CAPS scheme consists of a surface layer above the ground surface ($Z_{sfc} = 0$) and two soil layers below Z_{sfc}. Other versions of the scheme can provide an option of as many as 10 soil layers. The following text is devoted exclusively to the standard two-layer version. Figure 1 is a schematic of the scheme geometry. The ground surface is partially covered by vegetation (including natural vegetation such as trees, grass, and crops) with a fraction of σ_f and by bare soil with a fraction of $1 - \sigma_f$. The fractional coverage of vegetation, σ_f, is often referred to as the shading factor. The vegetation canopy coincides with the surface, which means that there is no resolved canopy layer in the scheme. Consequently, the CAPS scheme has no subcanopy flow dynamics or thermodynamics. It also implies that the skin surface temperature (T_{sfc}) represents both the bare soil surface temperature and the canopy temperature and that the displacement height related to vegetation is ignored in the scheme.

Above Z_{sfc} there is the atmospheric surface layer, which is usually the lowest model layer in a host atmospheric model. The altitude of the midlevel of the surface layer is denoted by Z_a and is usually of the order of 10^1 m, depending on vertical resolution of the host model. The atmospheric conditions (often called atmospheric forcing) are provided at Z_a. It is assumed that each of the energy fluxes and the water mass fluxes is constant within the surface layer. Here the energy fluxes include the solar shortwave radiation flux ($S\downarrow$), the atmospheric longwave radiation flux ($L\downarrow$), the turbulent sensible heat flux (H), and the turbulent moisture flux (E). The water mass fluxes include precipitation and dew/frost. The energy and water mass fluxes will be discussed later.

The two soil layers are composed of a thin upper layer ($Z_{sfc} - Z_1 = 5$ cm) and a thick lower layer ($Z_1 - Z_2 = 95$ cm), as indicated by Fig. 1. The temperature (T_1 and T_2) and the volumetric soil water content (Θ_1 and Θ_2) of the two soil layers are defined at the central points of the corresponding layers. The soil heat fluxes (G_0, G_1, and G_2) and the soil moisture fluxes (In, WF1, and WF2) are defined at the three interfaces of the two soil layers (see Fig. 1). Here, In is referred to as the infiltration rate. Conceptually, there is a third soil layer called subsoil layer ($Z_2 - Z_{bot}$) or bottom soil layer, which is below the lower soil layer. The temperature and the water content of the bottom soil layer designated as T_{bot} and Θ_{bot} are assumed to be invariant for a given location. For later use, we define the following notation:

$$H_1 = 2h_1 = Z_{sfc} - Z_1, \tag{1a}$$

$$H_2 = 2h_2 = Z_1 - Z_2, \tag{1b}$$

and

$$H_3 = 2h_3 = Z_2 - Z_{bot}. \tag{1c}$$

b. Turbulent fluxes at the surface

The surface fluxes of momentum (τ), sensible heat (H), and latent heat (Q) are parameterized as usual:

$$\tau = \rho_a u_*^2 = \rho_a C_m U_a^2, \tag{2}$$

$$H = \rho_a C_p C_h U_a(\theta_{sfc} - \theta_a), \tag{3}$$

and

$$Q = \mathrm{LE} = \rho_a L C_e U_a(q_{sfc} - q_a), \tag{4}$$

where ρ_a is the density of air, C_p is the specific heat for air, and L is the latent heat of vaporization or sublimation. The terms U_a, θ_a, and q_a are wind speed, virtual potential temperature, and specific humidity at Z_a. The corresponding surface values are θ_{sfc} and q_{sfc}. Finally, C_m, C_h, and C_e are the surface exchange coefficients for momentum, sensible heat, and moisture, respectively:

$$C_m = C_{mn} F_m(Z_a, Z_{om}, \mathrm{Ri}), \tag{5}$$

$$C_{mn} = k^2 \Big/ \left(\ln \frac{Z_a}{Z_{om}}\right)^2, \tag{5a}$$

$$C_e = C_h = C_{hn} F_h(Z_a, Z_{om}, Z_{oh}, \mathrm{Ri}), \tag{6}$$

and

$$C_{hn} = k^2 \Big/ \left[\mathrm{Pr} \ln\left(\frac{Z_a}{Z_{om}}\right) \ln\left(\frac{Z_a}{Z_{oh}}\right)\right], \tag{6a}$$

where k is the von Kármán constant, Pr is the neutral Prandtl number (1.0), and Z_{om} and Z_{oh} are the roughness length for momentum and sensible heat, respectively. The bulk Richardson number Ri for the surface layer is

$$\mathrm{Ri} = \frac{g Z_a(\theta_a - \theta_{sfc})}{\theta_a U_a^2}, \tag{7}$$

where g is the acceleration due to gravity (9.81 m s^{-2}). The term C_{mn} as defined by (5a) and C_{hn} as defined by (6a) are referred to as the neutral surface exchange coefficients (Ri = 0). The stability correction functions, F_m in (5) and F_h in (6), are specified by Mahrt (1987) for the stable case (Ri $>$ 0) and Louis et al. (1982) for the unstable case (Ri $<$ 0) as

$$F_m = e^{-m\mathrm{Ri}}, \qquad m = 1, \qquad \text{for Ri} > 0; \tag{8}$$

$$F_m = 1 - \frac{2b\,\mathrm{Ri}}{1 + 2bcC_{mn}\sqrt{(-\mathrm{Ri})Z_a/Z_{om}}}, \qquad \text{for Ri} < 0; \tag{8a}$$

$$F_h = e^{-m\mathrm{Ri}}, \qquad m = 1, \qquad \text{for Ri} > 0; \tag{9}$$

$$F_h = 1 - \frac{3b\,\mathrm{Ri}}{1 + 2bcC_{hn}\sqrt{(-\mathrm{Ri})Z_a/Z_{oh}}}, \qquad \text{for Ri} < 0; \tag{9a}$$

where

$$b = 5.0 \quad \text{and} \quad c = 7.5. \tag{10}$$

As indicated by (6), the surface exchange coefficient for moisture (C_e) is taken to be equal to C_h. It also implies that the roughness lengths for moisture (Z_{oe}) and for sensible heat (Z_{oh}) are taken as equal. As can be seen from (2)–(9), values for two sets of variables are needed in order to calculate the surface fluxes (τ, H, and Q). The first set includes Z_a, U_a, q_a, and θ_a, where θ_a is calculated from the temperature (T_a) and pressure (P_a) at Z_a. These variables are usually provided by separate prediction equations in a host atmospheric model or simply by an assigned forcing dataset. The second set of variables consists of Z_{om}, Z_{oh}, θ_{sfc}, and q_{sfc}, where Z_{om} and Z_{oh} are usually specified, and θ_{sfc}, or the corresponding T_{sfc} and the specific humidity at surface q_{sfc}, are determined via the surface energy balance equation and evaporation parameterization scheme that will be discussed below.

c. Surface energy balance and potential evaporation

The surface energy balance (SEB) equation plays a central role in the CAPS scheme. First, the SEB equation is used to calculate the potential evaporation (E_p) on which the parameterization of actual evapotranspiration (E) is based. Second, the SEB equation is used to calculate the surface sensible heat flux (H) through the use of the skin surface temperature (T_{sfc}) after E is determined. Third, the SEB equation serves to determine the snow melting rate, which will be discussed in the next section.

The SEB equation can be written as (e.g., Brutsaert 1982, chapter 6)

$$R_{\mathrm{net}} = (1 - \alpha)S\downarrow + \varepsilon L\downarrow - \varepsilon\sigma T_{\mathrm{sfc}}^4 = H + Q + G_0 + \mathrm{PF1} + \mathrm{PF2} + \mathrm{SF}, \tag{11a}$$

and

$$G_0 = k_T(\Theta_1)\frac{T_{\mathrm{sfc}} - T_1}{h_1}, \tag{11b}$$

where the nondimensional coefficient α in (11a) is the surface albedo, σ is the Stefan–Boltzmann constant, and ε is the ground surface emissivity. On the right-hand side of (11a), H and Q are the sensible and latent heat fluxes as defined by (3) and (4), respectively. The term G_0 is the soil heat flux at the surface, and k_T in (11b) is the soil thermal conductivity that depends on both soil water content Θ and soil type. The last three terms in (11a) are referred to as the precipitation-related heat fluxes. The term PF1 is related to the difference between the precipitation temperature and the surface temperature. The term PF2 is related to the phase change of the precipitated water. Table 1 lists the four types of precipitation and their corresponding expressions for PF1 and PF2. Note that the four precipitation types are mutually exclusive; that is, only one type of precipitation can occur at any one time. Also note that, given the precipitation intensity, PF1 depends on only ($T_{\mathrm{sfc}} - T_a$). The heat flux related to melting snow (see next section) is denoted as SF.

TABLE 1. The four types of precipitation and their related heat fluxes (PF1 and PF2) for the CAPS scheme. Prcp is the precipitation intensity. The terms T_{sfc} and T_a represent the surface and air temperature, respectively. The terms C_w and C_{snow} are the heat capacity for water and snow, respectively. The latent heat of fusion is denoted as L_f.

Precipitation type	Conditions	Precipitation-related heat flux
Rain	$T_a > 0$°C	PF1 = C_w Prcp ($T_{\mathrm{sfc}} - T_a$)
	$T_{\mathrm{sfc}} > 0$°C	PF2 = 0
Freezing rain	$T_a > 0$°C	PF1 = C_w Prcp ($T_{\mathrm{sfc}} - T_a$)
	$T_{\mathrm{sfc}} \le 0$°C	PF2 = $-L_f$Prcp
Sleet	$T_a \le 0$°C	PF1 = C_w Prcp ($T_{\mathrm{sfc}} - T_a$)
	$T_{\mathrm{sfc}} > 0$°C	PF2 = L_fPrcp
Snow	$T_a \le 0$°C	PF1 = C_{snow} Prcp ($T_{\mathrm{sfc}} - T_a$)
	$T_{\mathrm{sfc}} \le 0$°C	PF2 = 0

As mentioned at the beginning of this section, (11a) is first used to estimate E_p. The estimation of E_p closely follows Mahrt and Ek (1984). Actually, E_p can be defined by replacing q_{sfc} in (4) with $q^*_{\mathrm{sfc}}(T^*_{\mathrm{sfc}})$:

$$E_p = \rho_a C_e U_a [q^*_{\mathrm{sfc}}(T^*_{\mathrm{sfc}}) - q_a], \tag{12}$$

where q^*_{sfc} is the saturation specific humidity corresponding to a fictitious surface temperature T^*_{sfc}. On the other hand, from (4) and (11a) we have

$$\mathrm{LE}_p = R_{\mathrm{net}} - H - G_0 - \mathrm{PF1} - \mathrm{PF2} - \mathrm{SF}. \tag{13}$$

By using T^*_{sfc} instead of T_{sfc} for the terms in (13), the two equations, (12) and (13), have only two unknowns, E_p and T^*_{sfc}. Hence E_p can be evaluated given the forcing data and relevant parameters. When $E_p < 0$, a dewfall rate is defined as

$$\mathrm{Dew} = -E_p, \quad \text{for} \quad E_p < 0. \tag{14}$$

This dewfall rate will be added to the precipitation rate (Prcp, see Table 1) to calculate a total precipitation rate:

$$\mathrm{PR}_{\mathrm{total}} = \mathrm{Prcp} + \mathrm{Dew}. \tag{15}$$

d. Snow cover and snow melting

The ground surface may be covered by snow with a water equivalent snow depth S_d. The change in snow depth over time can be written as

$$\frac{\partial}{\partial t}S_d = \mathrm{PR}_{\mathrm{total}} - E_s - S_m, \tag{16}$$

where $\mathrm{PR}_{\mathrm{total}}$ has been defined by (15) and the two terms on the right-hand side of (15) should be referred to as snowfall and frost deposition rates. The E_s term in (16) is the sublimation over snow surface. The S_m term represents the snowmelt. Both S_d and S_m are defined in such a way that they cannot be negative. If $S_d = 0$, there is no snow melt ($S_m = 0$). For $S_d > 0$, S_m is related to SF in (11a) by

$$\mathrm{SF} = \rho_w L_f S_m, \tag{17}$$

where L_f is the latent heat of fusion and ρ_w is the water density.

To calculate S_m or SF, the following steps have been used: 1) calculate E_p and T^*_{sfc} from (12) and (13); 2) if the calculated $T^*_{\mathrm{sfc}} \le 0°\mathrm{C}$, then let $S_m = \mathrm{SF} = 0$ and $T_{\mathrm{sfc}} = T^*_{\mathrm{sfc}}$ (this means there is no net energy available for snow melt); and 3) if the calculated $T^*_{\mathrm{sfc}} > 0°\mathrm{C}$, then let $T_{\mathrm{sfc}} = 0°\mathrm{C}$ and calculate E_p and SF from (12) and (13) and calculate S_m from (17) (this means that the surface energy balance can provide net energy for snow melting and the surface temperature remains at the melting point (0°C) during snow melting). Under snow cover conditions, the equation for G_0 (11b) requires a modification. The actual snow depth can be expressed by h_s (Fig. 1) as

$$h_s = (\rho_w/\rho_s)S_d, \tag{18}$$

where ρ_s is the snow density. Currently, we use $(\rho_w/\rho_s) = 10$. The heat flux within the snow layer can be expressed as

$$G_s = k_s\frac{T_{\mathrm{sfc}} - T_{\mathrm{int}}}{h_s}, \tag{19}$$

where T_{int} is the temperature at the interface between the snow layer and the first soil layer and k_s is the thermal conductivity for snow, which depends on the porosity of snow (Gray and Male 1981). We choose the value of 0.13 W K^{-1} m^{-1} for k_s that corresponds to porosity of 0.8. The heat flux within the first soil layer can be written as

$$G_0 = k_T\frac{T_{\mathrm{int}} - T_1}{h_1}. \tag{20}$$

Under the assumption of $G_s = G_0$, T_{int} can be eliminated from (19) and (20). Consequently, we have

TABLE 2. General definitions for the five terms in Eq. (22).

	$S_d = 0$	$S_d > 0$
$E_p > 0$	Dew = 0 $E_s = 0$ $E_{\mathrm{soil}} > 0$ $E_{\mathrm{tr}} > 0$ $E_{\mathrm{ca}} > 0$	Dew = 0 $E_s = E_p$ $E_{\mathrm{soil}} = 0$ $E_{\mathrm{tr}} = 0$ $E_{\mathrm{ca}} = 0$
$E_p \le 0$	Dew = $-E_p$ $E_s = 0$ $E_{\mathrm{soil}} = 0$ $E_{\mathrm{tr}} = 0$ $E_{\mathrm{ca}} = 0$	Dew = $-E_p$ $E_s = 0$ $E_{\mathrm{soil}} = 0$ $E_{\mathrm{tr}} = 0$ $E_{\mathrm{ca}} = 0$

$$G_0 = G_s = k_T(\Theta_1)\frac{T_{\mathrm{sfc}} - T_1}{h_{\mathrm{eff}}} \tag{20a}$$

and

$$h_{\mathrm{eff}} = \left[1 + \frac{k_T}{k_s}\left(\frac{h_s}{h_1}\right)\right]h_1 = h_1 + \left(\frac{k_T}{k_s}\right)\left(\frac{\rho_w}{\rho_s}\right)S_d, \tag{21}$$

in which (18) has been used. The introduction of an effective depth (h_{eff}) for the ground heat flux (G_0) calculation under snow cover conditions is useful. In previous versions of the scheme, extremely large value of G_0 could occur due to very small h_s that could be as small as 10^{-5} m. Moreover, incredibly large values of surface sensible and latent heat fluxes were induced by the SEB equation when G_0 was extremely large. The use of (20a) and (21) can help avoid those ''spikes'' in surface energy flux estimation.

Finally, it should be pointed out that the albedo α in (11a) and the roughness length (Z_{om}, Z_{oh}) in (5), (6), (8a), and (9a) are highly dependent upon snow conditions. Many models, for example, Sellers et al. (1986) and Yang et al. (1997), have proposed different formulations for α and Z_{om} under various snow conditions.

e. Evapotranspiration parameterization

The CAPS scheme uses a general formulation for the total evapotranspiration at the surface (E),

$$E = (1 - \sigma_f)E_{\mathrm{soil}} + \sigma_f(E_{\mathrm{ca}} + E_{\mathrm{tr}}) + E_s - \mathrm{Dew}, \tag{22}$$

where E_{soil} is designated as the evaporation from the soil for the bare soil fraction, E_{tr} is the transpiration from the vegetation fraction, E_{ca} is the evaporation of precipitation intercepted by vegetation canopy (sometimes called interception loss), and E_s is the evaporation (sublimation) over the snow surface. The parameterization for the five components in (22) are based on E_p as well as on S_d. Table 2 gives general definitions for the five components. The parameterization for E_{soil}, E_{ca}, and E_{tr} for $E_p > 0$ and $S_d = 0$ are described as follows.

A particular approach to parameterize E_{soil} has been provided by Mahrt and Pan (1984). First, it calculates the surface soil water content Θ_{sfc} for a given positive E_p,

$$\Theta_{\text{sfc}} = \Theta_1 - h_1 \frac{E_p + K(\Theta_1)}{D(\Theta_1)}, \tag{23}$$

where Θ_1 is the volumetric soil water content for the first (upper) soil layer, $K(\Theta)$ is the hydraulic conductivity, and $D(\Theta)$ is the soil water diffusivity. Second, a specific parameter (Θ_{dry}) called air-dry value is introduced. Finally, E_{soil} is estimated based on a comparison between Θ_{sfc} and Θ_{dry},

$$E_{\text{soil}} = D(\Theta_1)\frac{\Theta_1 - \Theta_{\text{sfc}}}{h_1} - K(\Theta_1) = E_p, \quad \text{for } \Theta_{\text{sfc}} \geq \Theta_{\text{dry}}, \tag{24a}$$

and

$$E_{\text{soil}} = D(\Theta_1)\frac{\Theta_1 - \Theta_{\text{dry}}}{h_1} - K(\Theta_1) < E_p, \quad \text{for } \Theta_{\text{sfc}} < \Theta_{\text{dry}}. \tag{24b}$$

The evaporation of precipitation intercepted by the canopy is parameterized as

$$E_{\text{ca}} = E_p\left(\frac{C_w}{S}\right)^n, \quad \text{for } C_w \leq S \tag{25a}$$

and

$$E_{\text{ca}} = E_p, \quad \text{for } C_w > S, \tag{25b}$$

where C_w is the canopy water content, which is the amount of water that is captured and retained by the vegetation canopy (vegetal surface) and eventually evaporated back to the atmosphere without adding moisture to the soil. The term S is referred to as the water storage capacity (always positive) of the canopy, or the saturated value of C_w. A value of 0.5 for the exponent n in (25a) has been chosen by Pan and Mahrt (1987). Note that C_w is a function of time, whose value cannot exceed the value of S in a physical sense. Computationally, however, $C_w > S$ can occur. Once $C_w > S$, the excess water drips to the ground. For each time step, a drip index δ can be defined as

$$\delta = 1, \quad \text{when } C_w > S \tag{26}$$

and

$$\delta = 0, \quad \text{when } C_w \leq S.$$

With the help of this drip index, the canopy water budget can be written as

$$\frac{\partial C_w}{\partial t} = (1 - \delta)(\text{PR}_{\text{total}} - E_{\text{ca}}) \tag{27}$$

and

$$\text{DRIP} = \delta(\text{PR}_{\text{total}} - E_{\text{ca}}). \tag{28}$$

where Drip denotes the drip rate. Generally, $\delta = 1$ occurs for heavy precipitation and small water storage capacity of canopy.

The transpiration of vegetation is modeled as

$$E_{\text{tr}} = \sum_i E_{\text{tr}}(i) = \sum_{i=1}^{2} E_p P_c \left[1 - \left(\frac{C_w}{S}\right)^n\right]\left(H_i \Big/ \sum_i H_i\right) g(\Theta_i), \tag{29}$$

where P_c is the plant coefficient (sometimes called crop coefficient), a nondimensional fraction between zero and one, and i is the ith soil layer. The term P_c is formally defined here as the ratio of transpiration to the potential evaporation (E_p) for the case of dry canopy ($C_w = 0$) and sufficient soil water [$g(\Theta) = 1$]. The term P_c accounts for the various ways that stomatic, internal, and root resistances of vegetation influence the actual transpiration. In other words, P_c has absorbed all the complexity related to plant physiology in dealing with transpiration. In meteorological practice, the canopy resistance, r_c, instead of P_c, is frequently used. The relationship between P_c and r_c can be derived from the Penman–Montieth equation; see, for example, Eq. (17) in Xinmei and Lyons (1995). The factor $[1 - (C_w/S)^n]$ in (29) reflects the fact that transpiration is suppressed when water is retained on the vegetation canopy. If the canopy is totally covered by precipitated water ($C_w = S$), then the transpiration is completely suppressed. The last factor in (29) describes the dependence of transpiration on the soil water deficit represented by $g(\Theta)$,

$$g(\Theta) = \begin{cases} 1, & \text{for } \Theta > \Theta_{\text{ref}}, \\ (\Theta - \Theta_{\text{wilt}})/(\Theta_{\text{ref}} - \Theta_{\text{wilt}}), & \\ & \text{for } \Theta_{\text{wilt}} \leq \Theta < \Theta_{\text{ref}}, \\ 0, & \text{for } \Theta < \Theta_{\text{wilt}}, \end{cases} \tag{30}$$

where Θ_{wilt} and Θ_{ref} are two new parameters. Transpiration begins to decrease linearly when soil water content decreases below the reference value (Θ_{ref}). It ceases altogether when the soil water content is depleted below the wilting value Θ_{wilt}. In the current version of the model, the field capacity Θ_{fc} is used instead of Θ_{ref} in (30); see, for example, Jacquemin and Noilhan (1990).

f. Soil hydrological and thermodynamic equations

The hydrological equations for the two soil layers are

$$\frac{\partial}{\partial t}(H_1\Theta_1) = \text{In} - (1 - \sigma_f)E_{\text{soil}} - \sigma_f E_{\text{tr}}(1) - \text{WF1} \tag{31}$$

and

$$\frac{\partial}{\partial t}(H_2\Theta_2) = \text{WF1} - \text{WF2} - \sigma_f E_{\text{tr}}(2), \tag{32}$$

where In is the infiltration rate, and WF1 and WF2 are the soil water fluxes at the bottom of each of the two soil layers, respectively (positive downward, Fig. 1):

$$\mathrm{WF1} = \left[D(\Theta)\frac{\partial\Theta}{\partial z} + K(\Theta)\right]_{Z_1} \tag{33}$$

and

$$\mathrm{WF2} = [K(\Theta)]_{Z_2} = \mathrm{Drain}, \tag{34}$$

where $[\partial\Theta/\partial Z]_{Z_2} = 0$ has been assumed in (34).

The infiltration rate is given by

$$\mathrm{In} = \mathrm{PR}_{\mathrm{eff}} - \mathrm{Runoff}, \tag{35a}$$

$$\mathrm{Runoff} = \begin{cases} 0, & \text{if } \mathrm{PR}_{\mathrm{eff}} \le \mathrm{In}_{\max}, \\ \mathrm{PR}_{\mathrm{eff}} - \mathrm{In}_{\max}, & \text{if } \mathrm{PR}_{\mathrm{eff}} > \mathrm{In}_{\max}, \end{cases} \tag{35b}$$

and

$$\mathrm{In}_{\max} = \begin{cases} D(\Theta_{\mathrm{sat}})\dfrac{\Theta_{\mathrm{sat}} - \Theta_1}{h_1} + K(\Theta_{\mathrm{sat}}), & \text{for } \Theta_1 \le \Theta_{\mathrm{sat}}, \\ K(\Theta_{\mathrm{sat}}), & \text{for } \Theta_1 > \Theta_{\mathrm{sat}}, \end{cases} \tag{35c}$$

where Θ_{sat} is the saturation value of soil water content. The effective precipitation, $\mathrm{PR}_{\mathrm{eff}}$, is expressed as

$$\begin{aligned} \mathrm{PR}_{\mathrm{eff}} &= (1 - \sigma_f)\mathrm{PR}_{\mathrm{total}} + \sigma_f \mathrm{DRIP} \\ &= [1 - \sigma_f(1 - \delta)]\mathrm{PR}_{\mathrm{total}} - \sigma_f \delta E_{\mathrm{ca}}, \quad \text{for } S_d = 0 \end{aligned} \tag{36a}$$

and

$$\mathrm{PR}_{\mathrm{eff}} = S_m, \quad \text{for } S_d > 0. \tag{36b}$$

Here, (28) has been used for DRIP. The sum of (31) and (32) yields the water budget equation for the total soil water content W_s:

$$W_s = H_1\Theta_1 + H_2\Theta_2, \tag{37}$$

$$\frac{\partial W_s}{\partial t} = [1 - (1 - \delta)\sigma_f]\mathrm{PR}_{\mathrm{total}} - (1 - \sigma_f)E_{\mathrm{soil}} - \sigma_f E_{\mathrm{tr}} - \delta\sigma_f E_{\mathrm{ca}} - \mathrm{Runoff} - \mathrm{Drain}. \tag{38}$$

Multiplying (27) by σ_f and adding to (38), we have

$$\frac{\partial}{\partial t}(W_s + \sigma_f C_w) = \mathrm{Prcp} - E - \mathrm{Runoff} - \mathrm{Drain}. \tag{39}$$

Under snow cover conditions ($S_d > 0$), (31) and (32) are still applicable due to the assumptions in Table 2. However, (36b) should be used instead of (36a). Hence, from (34), (35a), and (36b), we have

$$\frac{\partial W_s}{\partial t} = S_m - \mathrm{Runoff} - \mathrm{Drain}. \tag{40}$$

Using (16) and (40), the water budget equation under snow cover condition can be expressed as

$$\frac{\partial}{\partial t}(W_s + S_d) + \mathrm{Prcp} - E - \mathrm{Runoff} - \mathrm{Drain}. \tag{41}$$

If a time domain had both a period with snow cover and a period without snow cover, (39) and (41) can be combined together to yield a unified total water budget equation such as

$$\begin{aligned} \frac{\partial}{\partial t}(W_{\mathrm{tot}}) &= \frac{\partial}{\partial t}(W_s + \sigma_f C_w + S_d) \\ &= \mathrm{Prcp} - E - \mathrm{Runoff} - \mathrm{Drain}. \end{aligned} \tag{42}$$

The integral budget of the W_{tot} for a time domain from t_1 to t_2 is

$$W_{\mathrm{tot}}(t_2) - W_{\mathrm{tot}}(t_1) = \int_{t_1}^{t_2} (\mathrm{Prcp} - E)\, dt - \int_{t_1}^{t_2} (\mathrm{Runoff} + \mathrm{Drain})\, dt. \tag{43}$$

The thermodynamic equations for the two soil layers are

$$\frac{\partial}{\partial t}(H_1 C_1 T_1) = G_0 - G_1 \tag{44}$$

and

$$\frac{\partial}{\partial t}(H_2 C_2 T_2) = G_1 - G_2, \tag{45}$$

where T_1 and T_2 are the soil temperatures for the first and second soil layers, respectively (Fig. 1). Here, C_i ($i = 1, 2$) is the volumetric heat capacity for the ith soil layer. Brutsaert (1982, section 6.3) has a detailed discussion on C_i. The soil heat flux in (44) and (45) can be expressed as

$$G_0 = k_T\frac{T_{\mathrm{sfc}} - T_1}{h_1}, \qquad G_1 = k_T\frac{T_1 - T_2}{h_1 + h_2},$$
$$G_2 = k_T\frac{T_2 - T_{\mathrm{bot}}}{h_2 + h_3}, \tag{46}$$

where k_T is the soil thermal conductivity, which depends on the soil moisture content (Θ).

The temperature of the bottom soil layer (T_{bot}) is assumed to be a constant. The prediction of the soil temperatures by (44) and (45) is performed by the use of the fully implicit Cranck–Nicholson scheme (Pan and Mahrt 1987). Note that under a snow cover condition, (20a) is used instead of the first equation of (46).

g. Soil and vegetation parameters

There are a number of parameters for the equations presented above. First, the hydraulic conductivity (K), the soil water diffusivity (D), and the soil thermal conductivity (k_T) can be related to soil moisture content and the soil moisture (matric) potential (Ψ) by the following equations:

TABLE 3. The four category parameters and their values used in the numerical simulation for Cabauw.

Parameters	Notation	Value for control run
Boundary condition parameters		
Roughness length for momentum	Z_{om}(m)	0.06 (snow free) 0.0024 (snow covered)
Roughness length for heat and moisture	Z_{oh}(m)	$0.1Z_{om}$
Surface albedo	α	0.23 (snow free) 0.75 (snow covered)
Thermal emissivity	ε	0.975
Bottom soil layer temperature	T_{bot}(k)	283.64
Initialization parameters		
Canopy water content	C_w (mm)	0.13
Soil temperature	T_1, T_2 (K)	279.0
Soil water content	Θ_1, Θ_2	0.468
Depth of snow	S_d (m)	0.0
Vegetation-related parameters		
Canopy water capacity	S (mm)	0.13
Shading factor	σ_f	0.956
Plant resistance	(r_c)min (s m^{-1})	30
Soil type	ST	#10 (silty clay)

$$K(\Theta) = K_{\text{sat}}(\Theta/\Theta_{\text{sat}})^{2b+3}; \tag{47a}$$

$$D(\Theta) = K(\Theta)\frac{\partial\Psi}{\partial\Theta} = -(bK_{\text{sat}}\Psi_{\text{sat}}/\Theta)(\Theta/\Theta_{\text{sat}})^{b+3}; \tag{47b}$$

$$\Psi = \Psi_{\text{sat}}(\Theta/\Theta_{\text{sat}})^{-b}; \tag{47c}$$

$$k_T(\Theta) = \begin{cases} 0.172, & P_f > 5.1, \\ 419\ \exp[-(2.7 + P_f)], & P_f \le 5.1; \end{cases} \tag{47d}$$

and

$$P_f = \log_{10}|\Psi|, \tag{47e}$$

where Ψ_{sat} and K_{sat} are the saturation values of Ψ and K, respectively. The term Θ_{sat} is the saturation volumetric moisture content, b is an empirical constant, and P_f is called the soil moisture tension. Equations (47a)–(47c) follow Clapp and Hornberger (1978), while (47d) and (47e) follow McCumber and Pielke (1981), and Al Nakshabandi and Hohnke (1965). Note that these four parameters (Ψ_{sat}, K_{sat}, Θ_{sat}, and b) depend on soil types. Next, with respect to evaporation formulation discussed in section 2e, there are an additional six parameters: σ_f, S, r_c, Θ_{wilt}, Θ_{fc}, and Θ_{dry}, of which the last three parameters are also soil-type dependent. The former three parameters are vegetation dependent.

1) VEGETATION-RELATED PARAMETERS

The fractional shading factor σ_f in (22) is simply the fraction of vegetation or fractional canopy cover. The term σ_f varies between 0 (no vegetation cover) and 1 (no bare soil, all ground surface covered by vegetation). In the CAPS scheme, σ_f has no direct relationship with radiative fluxes. It is, therefore, different from the shielding factor (Deardorff 1978; Pielke 1984). Here σ_f can be related to vegetation types and time of year (Dickinson et al. 1993).

The canopy water storage capacity S in (25) is expressed in depth of water, and it generally depends on meteorological conditions, vegetation types, and leaf or needle characteristics. Zinke (1967) provided an extensive review of S values. Average S values for various vegetation types range from 0.3 to 2.0 mm. A formulation to relate S with the leaf area index (LAI) such as

$$S = C_s\text{LAI} \tag{48}$$

has been suggested. For example, $C_s = 0.2$ mm was suggested by Wilson et al. (1987), $C_s = 0.1$ mm by Dickinson et al. (1993).

The canopy resistance (or surface resistance) r_c plays a key role in the parameterization of vegetation transpiration (E_{tr}) through (29). Here r_c depends on many factors including solar radiation, air temperature, atmospheric water vapor deficit, and soil moisture conditions (Jarvis 1976; Noilhan and Planton 1989; Jacquemin and Noilhan 1990). The interaction of these factors is quite intricate. In the current version of the model, following Jacquemin and Noilhan (1990),

$$r_c = \frac{(r_c)_{\min}}{\text{LAI}\, f_1 f_2 f_3 f_4}, \tag{49}$$

where $(r_c)_{\min}$ is the minimum value of the surface resistance and f_i ($i = 1, 4$) represents the effects of solar radiation (f_1), air temperature (f_2), air humidity deficit (f_3), and soil moisture (f_4), respectively. Actually, the effect of soil moisture (f_4) has already been included by $g(\Theta)$ [see (30)] for E_{tr}. Therefore, $f_4 = 1$ for the CAPS scheme. Lastly, it should be pointed out that the albedo (α) and the roughness length (Z_{om}) should also be vegetation-related parameters (e.g., Wilson et al. 1987, Table 3).

2) SOIL-RELATED PARAMETERS

There are seven parameters (Θ_{sat}, Ψ_{sat}, K_{sat}, b, Θ_{wilt}, Θ_{fc}, and Θ_{dry}) that are related with soil hydrology and

soil thermodynamics through (24), (30), and (47), and depend upon soil types. As has been done by many authors (Clapp and Hornberger 1978; Pielke 1984; Wetzel and Chang 1987; Garratt 1992), 11 soil types have been used for the CAPS scheme.

The values of the first five parameters (Θ_{sat}, Ψ_{sat}, K_{sat}, b, Θ_{wilt}) have been given by Garratt (1992, Table A9). The Θ_{fc} values can be found from Table 1 of Jacquemin and Noilhan (1990). Another set of the values of these six parameters are also given by Wetzel and Chang (1987) based on Cosby et al. (1984). The two sets of values, especially the Ψ_{sat} values, are significantly different from each other. Ek and Cuenca (1994) have shown that even the average values of these parameters should be used with caution if standard deviations of their values are large. In our experiment, the values of the six parameters provided by Wetzel and Chang are used.

As for the air-dry value (Θ_{dry}), careful consideration is needed since the use of Θ_{dry} for soil evaporation (E_{soil}) parameterization represents a unique approach that is different from other existing approaches (Garratt 1992; Lee and Pielke 1992). As discussed by Hillel (1982, 275–281), Θ_{dry} can be defined as the lower limit of surface soil moisture. Such a definition of Θ_{dry} has been used by Hanks et al. (1969), Nimah and Hanks (1973), and Feddes et al. (1974). An alternative method to deduce Θ_{dry} is to use (47c),

$$\Theta_{dry} = \Theta_{sat}(\Psi_{dry}/\Psi_{sat})^{-1/b} \quad (50)$$

and

$$\Psi_{dry} = (R_v T_{sfc}/g) \ln(\mathrm{RH}), \quad (51)$$

see for example, Philip (1957), where R_v is the gas constant for water vapor, T_{sfc} is the soil surface temperature, g is the gravity acceleration, RH is the relative humidity of the air adjacent to the water in the soil pore at soil surface. Kondo et al. (1990) have stressed the difference between this relative humidity (RH) and the relative humidity in the surface air just above the ground. The air-dry term Θ_{dry} appears not to be sensitive to either T_{sfc} or RH (Garratt 1992, Fig. 5.9; Kondo et al. 1990, Fig. 5). The calculated values from (50) and (51) for different soil types under the assumption of T_{sfc} = 280 K and RH = 5% are used in the current version of the CAPS scheme.

3. Design of the numerical experiment

The purpose of the numerical experiment is to evaluate the performance of the CAPS scheme with the help of the Cabauw data and hence to achieve a better understanding of the scheme's physics. In this section, the experimental method and approach (section 3a), the Cabauw dataset (section 3b), and the specification of relevant parameters (section 3c) are described. The results of this numerical experiment will be the subject of the next section.

a. Experimental method and approach

Following the general methodology of PILPS phase 1a (Pitman et al. 1993) and phase 2a (Chen et al. 1997), the numerical experiment has been conducted as an offline (''stand-alone'' or ''zero-dimensional'') experiment, where atmospheric forcing data are externally prescribed. This means no feedbacks occur between the land surface and the atmosphere. This method has the advantage of disinvolvement in complex feedback effects (Jacobs and DeBruin 1992; Viterbo and Beljaars 1995). Consequently, it is easier to interpret results from offline experiments than from complicated interactive (coupled) experiments. The offline simulation (or the control simulation) is driven by the atmospheric forcing data from Cabauw with specified values of relevant parameters. The Cabauw data have been provided from 1 January to 31 December of 1987. The control run is initialized at 1 January 1987 and is run to equilibrium by looping through the one year's forcing as many times as necessary. Equilibrium is achieved when the monthly mean surface fluxes (latent heat flux and sensible heat flux) do not change by more than 0.1 W m^{-2} from January of year n to January of year $n + 1$. For the CAPS scheme, usually an equilibrium can be reached when $n = 2$ (total integration time of 17 520 h or 2 yr). Results from the control simulation have been compared against the Cabauw validation data to evaluate the scheme's performance.

b. Cabauw data

The micrometeorological data used in this study as well as in PILPS phase 2a experiments are based on measurements and observations on a 213-m meteorological tower at Cabauw (51°58′N, 4°56′E) in the central Netherlands during 1987. The Cabauw site is located on flat terrain. It consists mainly of grassland interrupted by narrow ditches. The soil consists of a clay layer about 70 cm deep on top of a peat layer about 7 m deep. The 1987 Cabauw dataset was kindly provided by the Royal Netherlands Meteorological Institute (KNMI). Beljaars and Bosveld (1997, hereafter referred to as BB97), have presented detailed information about the 1987 Cabauw dataset (release 2). The release 2 data represent an improvement over the release 1 data that were used by Beljaars and Viterbo (1994). Most recently, release 3 of the 1987 Cabauw dataset is available. Release 3 is the same as release 2 except for a correction in rainfall as described by Beljaars (1995). Therefore, the current study uses the newly revised release 3 Cabauw dataset.

The Cabauw data are provided at 30-min intervals (all quantities are averages for 30 min) for the entire year of 1987. It consists of both atmospheric forcing data and validation data. Altogether, the data contain time series for 19 meteorological and soil variables. There are eight forcing variables: downward solar radiation, downward (atmospheric) thermal radiation,

TABLE 4. The CAPS scheme simulated monthly and yearly averages of surface energy balance, Eq. (11a) for Cabauw 1987. All terms are in W m^{-2}. The bottom line shows the observed values.

Month	R_{net}	H	Q	G_0	PF1	PF2	SF	Residual
Jan	−15.361	−14.649	5.382	−6.075	−0.007	−0.156	0.000	0.143
Feb	0.471	−7.174	8.164	−0.641	−0.001	−0.050	0.131	0.041
Mar	20.220	4.017	19.497	−3.133	0.000	0.000	0.000	−0.196
Apr	71.648	4.637	62.920	4.320	0.000	0.000	0.000	−0.229
May	92.118	22.329	70.152	−0.176	0.000	0.000	0.000	−0.186
Jun	88.248	15.608	69.215	3.584	0.000	0.000	0.000	−0.160
Jul	105.929	20.254	82.192	3.761	0.000	0.000	0.000	−0.278
Aug	78.820	6.532	69.918	2.642	0.000	0.000	0.000	−0.273
Sep	44.846	−4.919	49.995	0.087	0.000	0.000	0.000	−0.317
Oct	7.954	−19.345	28.998	−1.340	0.000	0.000	0.000	−0.358
Nov	−8.780	−15.611	11.999	−4.863	0.000	0.000	0.000	−0.305
Dec	−15.654	−17.906	4.176	−1.698	−0.006	−0.086	0.159	−0.292
Year	39.416	−0.469	40.390	−0.302	−0.001	−0.024	0.025	−0.202
Observed	40.73	0.98	40.97	−0.55	—	—	—	—

large-scale precipitation (RAINL), convective precipitation (RAINC), wind speed, wind direction, air temperature, and specific humidity. The measurement taken for the last four variables are at a 20-m height. For the CAPS scheme, the wind direction is not used and a precipitation rate for each time step can be calculated from the sum of RAINC and RAINL.

The Cabauw validation data include friction velocity (u_*), sensible heat flux (H), latent heat flux (Q), net total radiation (R_{net}), ground heat flux at the surface (G_0), and surface soil temperature (T_{so}). However, T_{so} is less suitable than radiative surface temperature due to exposure and representativeness problems. On the other hand, the radiative surface temperature (T_{rad}) can be calculated from the upward and downward thermal radiations and can be compared with the simulated T_{sfc} of the scheme. Therefore, six quantities (u_* H, Q, R_{net}, G_0, and T_{rad}) from the Cabauw validation data have been used for this validation study. The validation data also include the error bounds around observations for monthly means of H, Q, R_{net}, and G_0. These error bounds, however, are rough estimates only. Finally, the assumption is made that the offline simulations are comparable with point observations such as Cabauw data (Chen et al. 1997).

c. Parameters and their values

A number of parameters are involved in the CAPS scheme, as seen from section 2. They can be broadly divided into the internal and external groups. The former include two categories: vegetation-related and soil-type-related parameters that have been qualitatively discussed in the last section. The latter include three categories: atmospheric forcing (driving), boundary condition, and initialization parameters. Among the five categories, the atmospheric forcing parameters are provided by the Cabauw forcing data as discussed above. The parameter values for the other four categories are listed in Table 3.

The values of most parameters in Table 3 are the recommended values by PILPS. These values were derived from a variety of sources in an attempt to fully characterize the Cabauw site (Chen et al. 1997). It should be pointed out, however, that these suggested values may not necessarily be representative. Representative values of a complete set of site-specific parameters are extremely difficult to acquire due to limitations of measurements and observations, and surface inhomogeneity. The roughness length for momentum (0.06 m) is an averaged value based on Table 3 in BB97. The one order of magnitude difference between Z_{oh} and Z_{om} in Table 3 is our best estimate. The albedo value ($\alpha = 0.23$) is the value used by Beljaars and Viterbo (1994). A typical emissivity for grassland, $\varepsilon = 0.975$, is assumed since there was no observation for ε at Cabauw. Based on BB97, a rough estimate of the minimum canopy resistance, $(r_c)\text{min} = 30$ s m^{-1} has been made. The value of T_{bot} has not been suggested by PILPS. The yearly average value of the soil temperature at 2 cm (283.64 K) from Cabauw data has been assumed based on the consideration that yearly averages of ground heat fluxes as measured at Cabauw are very small (less than 0.5 W m^{-2}).

4. Results of the numerical experiment

a. Results of consistency tests

As required in the PILPS experiments for phase 2a (Chen et al. 1997), outputs from a scheme should first be checked to ensure the conservation of energy and water. This requirement is absolutely necessary since it is extremely difficult, if not impossible, to know whether or not a scheme's algorithms are valid. Table 4 gives the CAPS scheme simulated monthly and yearly averages of the components in the surface energy balance equation (11a), with the residual defined as the difference between the left- and the right-hand sides of the equation. Table 4 shows that the magnitudes of the residuals for those monthly and yearly averages are small-

TABLE 5. The CAPS scheme simulated monthly and yearly water balance, Eq. (43) for Cabauw 1987. All terms are in mm (water). The bottom line shows the observed values. The precipitation term is not simulated.

Month	Change of water	Precipitation	Evaporation	Runoff	Drainage	Residual
Jan	−16.701	55.530	5.766	0.000	66.465	0.000
Feb	8.960	33.390	7.901	0.000	16.415	−0.115
Mar	8.938	99.740	20.888	0.000	69.670	−0.244
Apr	−49.454	33.850	65.236	0.000	18.068	0.000
May	19.677	101.070	75.158	0.000	6.234	0.000
Jun	2.774	93.210	71.762	0.875	17.799	0.000
Jul	15.616	109.120	88.057	0.979	4.468	0.000
Aug	−6.056	86.110	74.908	0.000	17.259	0.001
Sep	−8.980	61.600	51.835	9.618	9.128	0.000
Oct	24.671	117.440	31.067	0.000	61.701	0.000
Nov	0.153	92.100	12.440	0.000	79.507	0.001
Dec	0.402	48.080	4.473	0.000	43.080	−0.124
Year	0.00	931.24	509.49	11.47	409.79	−0.48
Observed	—	931.23	516.81	—	—	—

er than 0.4 W m^{-2}, which is much smaller than the required value of 3 W m^{-2} for PILPS. Table 4 also shows that the precipitation-related energy fluxes are insignificant as compared to other terms in (11a). The yearly averages of the four significant terms (R_{net}, H, Q, and G_0) in (11a) are in good agreement with the yearly averages of the Cabauw observations. Table 5 provides CAPS scheme simulated monthly and yearly averages of the components in the water balance equation (43), with the residual defined as the difference between left- and right-hand sides of the equation. The magnitudes of the residuals in Table 5 are smaller than 0.5 mm water, which is much less than the required value of 3 mm for PILPS. The monthly averaged runoff appears to be negligible except for September 1987. For yearly averages, the precipitation is nearly balanced by the total evaporation and drainage. A further check of the water conservation in the partition of total evaporation is provided by Table 6, which shows the five components in (22). Table 6 clearly indicates that (22) is satisfied. It also demonstrates that the evaporation over a snow surface and the dew are usually small at Cabauw, as compared with other terms in (22). Generally, the evapotranspiration (E_{tr}) is the dominant term for total evaporation at Cabauw. This is no surprise because the land surface at Cabauw is almost wholly covered by vegetation ($\sigma_f = 0.956$). In summary, the three tables above demonstrate that the physical constraints of energy and water conservation have been satisfactorily met in the CAPS scheme, indicating internal consistency.

b. *Comparison of surface fluxes and important variables*

The following comparison of various surface fluxes and related variables between the CAPS scheme simulation for an equilibrium year and the Cabauw 1987 observations are organized in the same sequence as is followed in the CAPS scheme algorithm. We will focus on two aspects of those fluxes and variables: their seasonal variations (monthly averages) and diurnal variations (averaged over a whole year), as in PILPS (Chen et al. 1997).

1) MOMENTUM FLUX

As seen from (2), (5), and (5a) that u_* is determined by U_a and C_m, the latter is a function of C_{mn} and F_m or

TABLE 6. The CAPS scheme simulated monthly and yearly averages of the five components for the total evapotranspiration, Eq. (22), and the potential evaporation (E_p). All terms are in W m^{-2}.

Month	$(1 - \sigma_f)E_{soil}$	$\sigma_f E_{tr}$	$\sigma_f E_{ca}$	E_s	Dew	E	E_p
Jan	0.57	0.84	2.81	1.88	0.72	5.38	14.10
Feb	0.96	4.53	2.62	0.91	0.86	8.16	21.82
Mar	2.46	11.12	6.55	0.16	0.79	19.50	55.20
Apr	4.14	54.63	4.85	0.00	0.70	62.92	98.42
May	4.78	58.89	7.20	0.00	0.71	70.15	109.39
Jun	4.23	58.20	7.54	0.00	0.75	69.22	95.38
Jul	4.16	72.25	6.75	0.00	0.97	82.19	127.88
Aug	4.20	59.37	7.46	0.00	1.11	69.92	94.28
Sep	3.16	43.77	5.73	0.00	2.66	49.99	69.06
Oct	2.17	22.33	6.59	0.00	2.09	29.00	47.19
Nov	1.03	5.56	6.42	0.00	1.01	12.00	22.46
Dec	0.67	1.98	2.49	0.21	1.18	4.18	14.33
Year	2.72	32.94	5.60	0.26	1.13	40.39	64.39

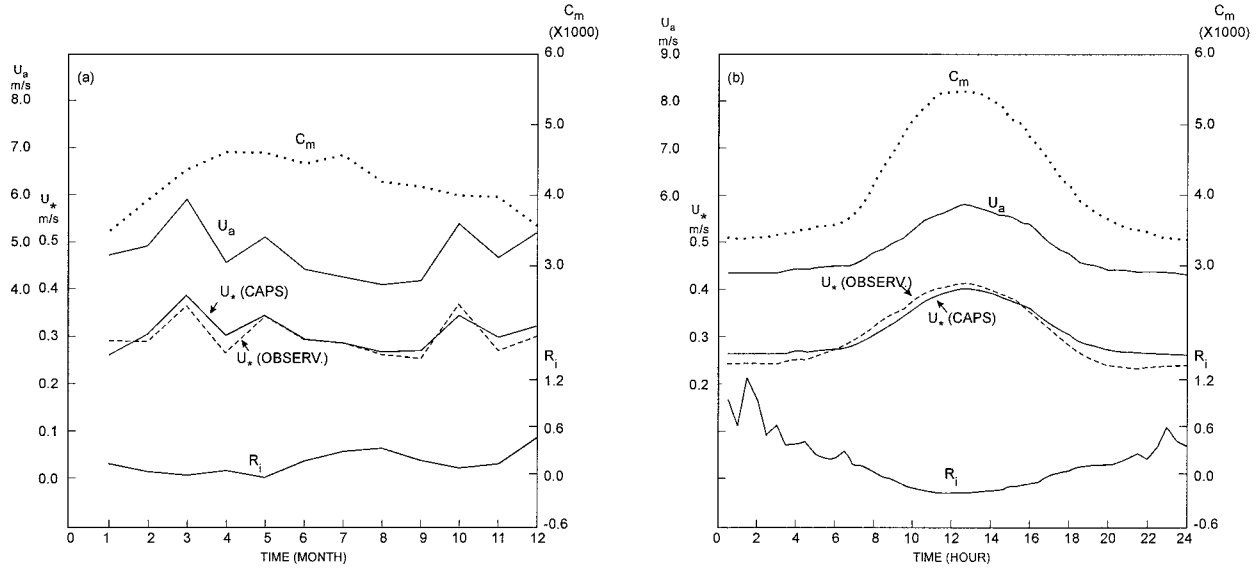

FIG. 2. (a) Seasonal and (b) diurnal (averaged over 1 yr) variations of surface exchange coefficient for momentum (C_m), observed wind speed (U_a) at 20-m height, simulated (solid line) and observed (dashed line) friction velocity (u_*), and Richardson number (Ri) given by Eq. (7). Notice the different scales for those four variables.

Z_{om} and Ri. Figures 2a,b show the seasonal and diurnal variations for u_* as well as its related variables U_a, C_m, and Ri. Figure 2a illustrates that U_a, the observed monthly averaged wind speed, fluctuates from month to month during 1987 with a maximum speed of 5.95 m s^{-1} for March and a minimum speed of 4.14 m s^{-1} for August. The bulk exchange coefficient for momentum, C_m, has a relatively smooth annual cycle with a maximum of 0.004 63 for May and a minimum of 0.003 46 for January. The seasonal variation of Ri is basically in opposite phase with that of C_m. The seasonal variation of u_* appears to follow that of U_a. This is due to the dominating effect of U_a and minor effect of C_m on u_*. Figure 2b illustrates that U_a has a well-defined and smooth diurnal variation with a maximum of 5.82 m s^{-1} at noon and a minimum of 4.34 m s^{-1} at midnight. The diurnal variation of C_m is also well defined and is in phase with that of U_a. On the other hand, the diurnal variation of Ri is 180° out of phase with that of C_m. As in the seasonal variation (Fig. 2a), the diurnal variation of u_* closely follows that of U_a due to its dominating effect.

As seen from both Figs. 2a and 2b, in comparison with the Cabauw observations, the CAPS scheme has simulated the seasonal and diurnal variations of u_* well. The annual mean of u_* from the scheme is 0.311 m s^{-1} as compared to 0.303 m s^{-1} from Cabauw observations. The slight overestimation by the CAPS scheme may result from the constant value of Z_{om} (6 cm) for the simulation. Actually, Z_{om} depends on wind direction (BB97). The yearly averaged value of Z_{om} weighted by wind direction at Cabauw for 1987 is 5.73 cm. A detailed comparison of u_* between simulation and observation from Fig. 2a shows that u_* appears to be overestimated for most months except for January and October. The underestimation of u_* for January is probably related to snow cover. The simulation yields a snow cover of 11 days (from 7 to 17) in January. It is not clear whether the CAPS scheme has overpredicted snow cover or that assigned roughness length (2.4 mm) for momentum under snow cover is too small. There was no reliable information about snow from the 1987 Cabauw dataset. Also note that there is no error estimation for u_* in the Cabauw data. A ±10% error in u_* deduced from observations is not impossible. On the other hand, Fig. 2b indicates that u_* appears to be overestimated from afternoon (1600 UTC) to early morning (0400 UTC) when Ri > 0. This implies that the stability correction function F_m in (8) could have been overestimated. The simulated u_* under stable stratification (Ri > 0) could have been smaller if we had adopted a larger value of m in (8), as originally suggested by Mahrt (1987), although there is no formal justification for doing this.

2) LATENT HEAT FLUX (LE)

Figures 3a,b show the seasonal and diurnal variations for Q, Q_p, C_e, and W_s. As discussed in section 2e, the evapotranspiration (E) has been parameterized according to the potential evaporation (E_p). Figure 3a shows that the potential latent heat flux Q_p (=LE_p) has a large annual cycle with a maximum Q_p of 127.9 W m^{-2} in July and a minimum Q_p of 14.1 W m^{-2} in January. The dip in June is primarily due to the annual cycle of downward shortwave radiation at Cabauw, which has a dip of more than 20 W m^{-2} in June [see Fig. 1 of Chen et al. (1997)]. A slight dip of C_e in June contributed as

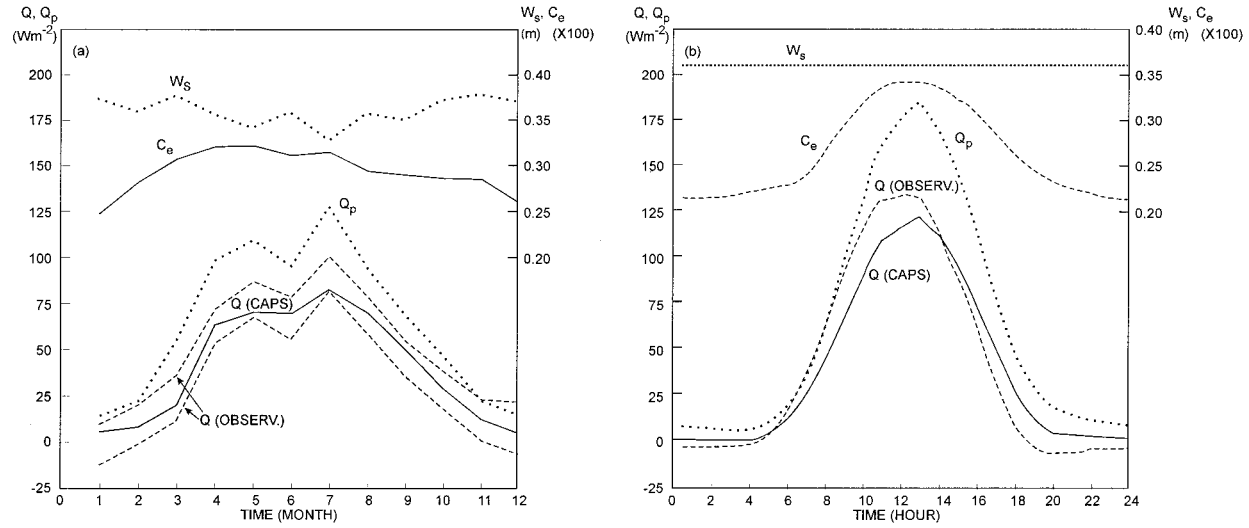

FIG. 3. (a) Seasonal and (b) diurnal (averaged over 1 yr) variations of total soil water content (W_s), surface exchange coefficient for moisture (C_e), latent heat flux corresponding to the potential evaporation (Q_p), and simulated (solid line) and observed (dashed line) latent heat flux (Q). The two dashed lines in (a) indicate the upper- and lower-error bonds of the observed Q.

well. The annual variation of latent heat flux (Q) closely follows that of Q_p as seen from Fig. 3a. The two dashed lines in the figure give the upper- and lower-error bounds around the observed Q. A comparison of Q between the simulation and Cabauw observations indicates that the CAPS scheme has generally predicted the monthly averages of Q well. All of the 12 monthly averages fall within the error bound. The CAPS scheme, on the other hand, produces relatively large deviations for a few months. For example, the scheme predicted 82.19 W m^{-2} for July, while the observed value was 90.97 W m^{-2}, with the error bound between 100.97 and 80.97 W m^{-2}. It is not clear whether this underprediction is related to the lowest total soil moisture content (W_s) in July predicted by the scheme. The Cabauw data, unfortunately, provide no soil moisture content. Also for July, the simulated ratio of the interception evaporation (E_{ca}) to the total evaporation (E) is only 8.2%, while this ratio is 13.9% for the entire year of 1987 (Table 6). The annual ratio of E_{ca} to E, as reported by BB97, could be 31% as simulated by the ECMWF land surface scheme. It is extremely difficult to validate the E_{ca} term as well as the other four terms in Eq. (22) separately.

Figure 3b shows that Q_p, Q, and C_e all have similarly pronounced diurnal cycles with maxima around noon and minima around midnight. The diurnal variation of actual evapotranspiration (Q) basically follows that of potential evaporation (Q_p). A comparison of Q between the simulation and Cabauw observations indicates that Q appears to be underpredicted in the morning and early afternoon, while it is overpredicted during the rest of the day. This situation is very similar to the situation for u_* shown in Fig. 2b. The underestimation or overestimation of u_* could be related to the bulk transfer coefficient for momentum (C_m). Likewise, the underestimation or overestimation of the latent heat flux in the diurnal cycle could be related to C_e and hence C_m since C_e is proportional to C_m. However, the situation for the latent heat flux prediction is more complicated than that for momentum flux prediction. Here, a less accurate estimation of C_e would first affect E_p, and subsequently the prediction of E or Q would suffer. At present, it is uncertain how serious E_p had been overpredicted or underpredicted by the CAPS scheme. In addition, the diurnal variation of the canopy resistance can be large (see Fig. 11 of BB97), but this quantity is difficult to validate.

3) SURFACE RADIATIVE TEMPERATURE

Figures 4a,b present the seasonal and diurnal variations for the surface radiative temperature T_{rad}, referred to as skin temperature (T_{sfc}) in the CAPS scheme. The T_{sfc} term has been calculated from surface energy balance Eq. (11a) after Q is determined. It is obvious that any error in the estimation of other terms in (11a) has a direct effect on the T_{sfc} estimation. On the other hand, the Cabauw observation has included soil surface temperature $T_s(z = 0)$, which was measured by a nickel resistance thermometer. Here T_s can hardly be considered representative of T_{rad}. The inclusion of T_s in Fig. 4 is for general information only. The term T_s appears to be always greater than T_{rad} by 2–4 K, as indicated by Fig. 4. Two values (1.00, 0.95) of ε have been assumed to evaluate T_{rad} since there was no observation of ε at Cabauw.

Figure 4a shows that both the simulated (T_{sfc}) and observed (T_{rad}) radiative surface temperatures have a regular seasonal cycle. The annual averages for T_{sfc} and T_{rad} with $\varepsilon = 1.0$ and 0.95 are 281.64, 280.64, and

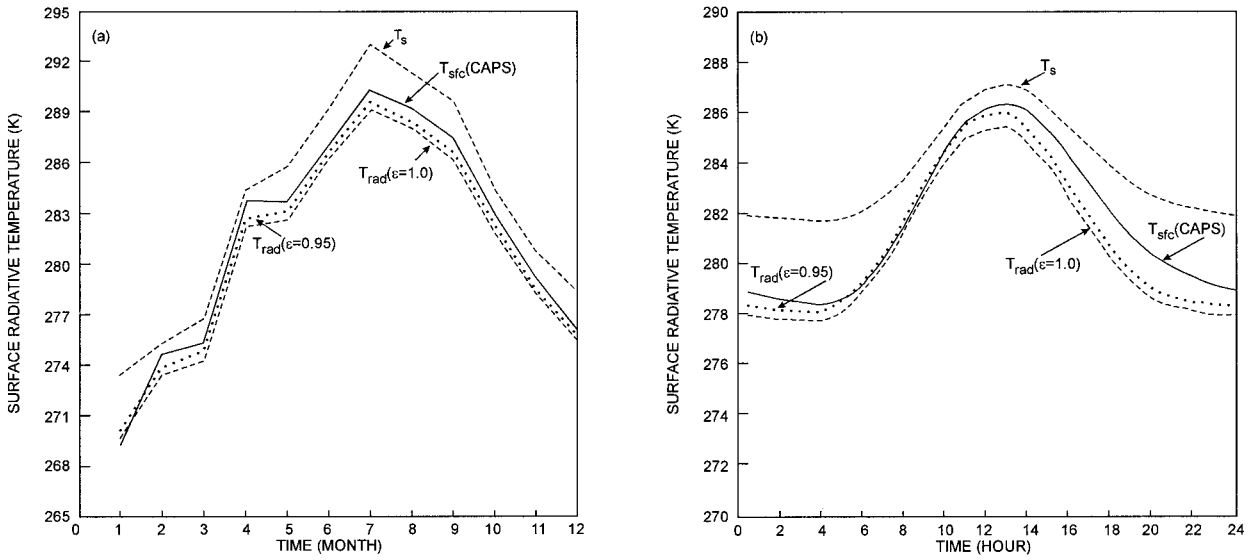

FIG. 4. (a) Seasonal and (b) diurnal (averaged over 1 yr) variations of measured soil surface temperature (T_s), and simulated (T_{sfc}) and observed (T_{rad}) surface radiative temperature with assumed emissivity (ε).

281.08 K, respectively. The monthly averages of T_{sfc} are about 0.5–1.4 K greater than those of T_{rad} except for January, for which T_{sfc} is about 0.6 K smaller than T_{rad}. This exceptionally smaller T_{sfc} seems to be related to the snow cover simulation. Under the snow cover situation, the albedo (α) has been assumed to be 0.75. The monthly average of α for January has been computed as 0.401. This large value of α seems responsible for the lower estimation of T_{sfc} for January.

Figure 4b illustrates smooth diurnal variations for both T_{sfc} and T_{rad}. As in the seasonal variation (Fig. 4a), T_{sfc} is almost always greater than T_{rad}. The simulated T_{sfc} as compared to the observed T_{rad} appears particularly good in the middle of the morning. The closeness between the simulated and observed T_{rad} for this period has also been observed in other schemes in PILPS.

4) SURFACE NET RADIATION

The seasonal and diurnal variations of surface net radiation (R_{net}) are presented by Figs. 5a,b. The CAPS scheme computes R_{net} from (11a) after T_{sfc} has been determined. The observed R_{net} is based on direct measurement by the net radiation instrument with a correc-

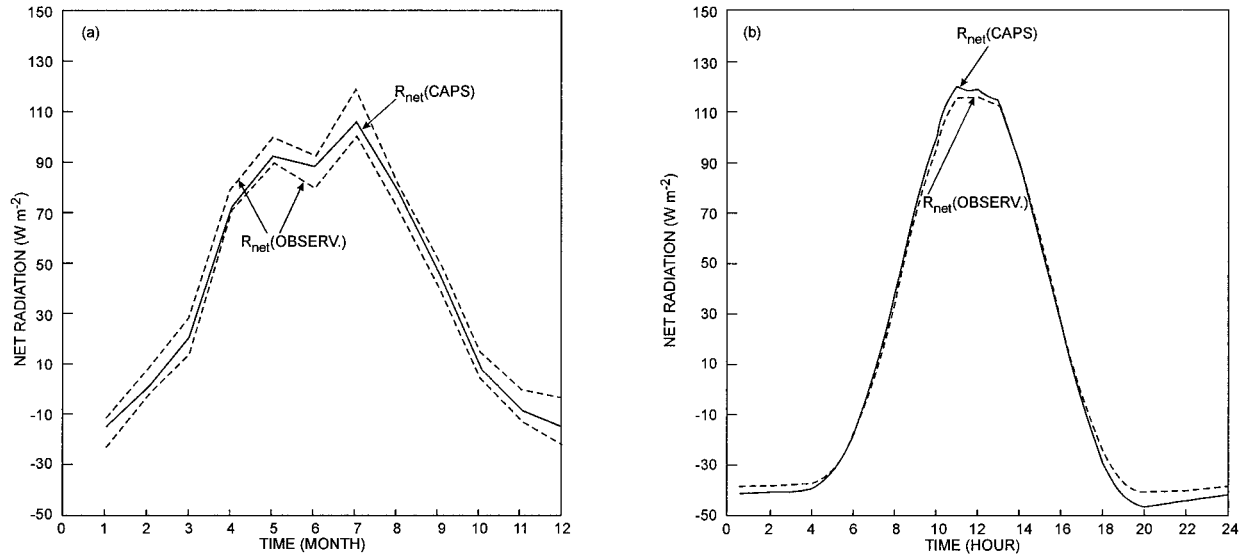

FIG. 5. (a) Seasonal and (b) diurnal (averaged over 1 yr) variations of simulated (solid line) and observed (dashed line) surface net radiation (R_{net}). The two dashed lines in (a) indicate the upper- and lower-error bonds of the observed R_{net}.

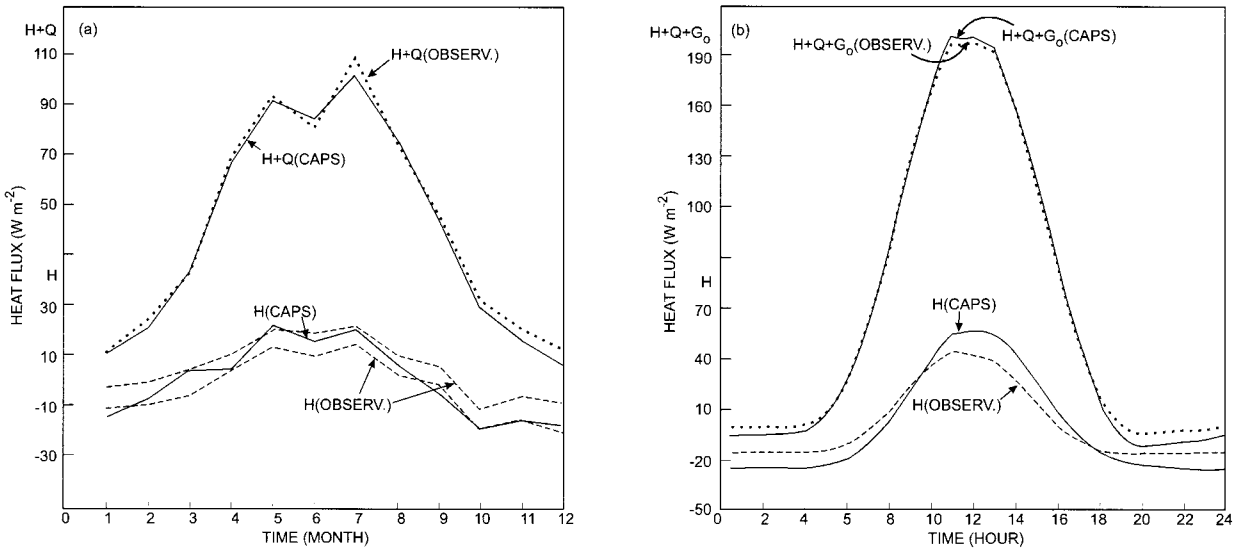

FIG. 6. (a) Seasonal and (b) diurnal (averaged over 1 yr) variations of simulated (solid line) and observed (dashed line) sensible heat flux (H), the sum of H and Q in Fig. 6a, and the sum of H, Q, and G_0 in (b). The terms Q and G_0 denote the latent and ground heat flux, respectively. The two dashed lines in (a) indicate the upper- and lower-error bonds of the observed H.

tion as described by BB97. The two dash lines in Fig. 5a indicate the upper- and lower-error bounds around the observed values of R_{net}. As shown by Fig. 5a, the simulated monthly averages of R_{net} do not differ from the observations by more than the estimated maximum errors. This demonstrates that the scheme has generally predicted monthly averages of R_{net} very well. However, the simulated monthly average for January (-15.36 W m^{-2}) is larger than the observation (-17.74 W m^{-2}), and those for April (71.65 W m^{-2}) and July (105.93 W m^{-2}) are smaller than the observations (75.05 and 113.75 W m^{-2}, respectively). This overestimation for January and the underestimation for April and July are probably related to the corresponding estimations of T_{sfc} for those months as seen from Fig. 4a.

Figure 5b shows that R_{net} has a large amplitude in its diurnal cycle. Generally, the simulated R_{net} is a little larger than the observed R_{net} in daytime (0530–1500 UTC) and a little smaller in the rest of the day, with a deviation of less than 9 W m^{-2}. This is also probably related to the diurnal variation of T_{sfc}, as shown in Fig. 4b. It is interesting to note that, similar to the CAPS scheme, many other schemes in PILPS have over- and underpredicted R_{net} with a similar pattern in both seasonal and diurnal variations (see Figs. 3a and 3b in Chen et al. 1997). It is still a challenge to physically explain such a pattern in the schemes' performance.

5) SENSIBLE HEAT FLUX (H)

Figure 6 shows the seasonal and diurnal variations for sensible heat flux (H). The two dashed lines in Fig. 6a are the upper- and lower-error bounds around the observed H. The seasonal variation of H ranges from -20.0 to 23.0 W m^{-2}. The deviations of the simulated monthly means from observations vary from -7.7 (January) to 5.2 W m^{-2} (May). These deviations result primarily from errors in the latent heat flux estimations (Fig. 3a). For example, Q has been overestimated by 7.1 W m^{-2} for January. This overestimation results in an underestimation of 7.7 W m^{-2} in H for January. Likewise, Q has been underestimated by 6.8 W m^{-2} for May, which induces an overestimation of 5.2 W m^{-2} in H for that month. To further illustrate the close relationship between Q and H estimations, Fig. 6a has two curves for the observed and simulated sums of Q and H. It shows that the two curves are close to each other. If there were small errors in the estimation of Q, then there should have been small errors in the H estimation. On the other hand, a comparison of these two curves shows that there are still some discrepancies between them. For example, the discrepancy in July is due to the underestimation of Q, which can be seen from Fig. 3a and has been discussed earlier. In December, the discrepancy between simulation and observation is believed to be due to the underestimation of H under stable atmospheric conditions, as will be discussed below.

Figure 6b shows that for diurnal variation the CAPS scheme has overestimated H during the day (from 0930 to 1730 UTC), while underestimating H the rest of the day. The maximum overestimation is 16.8 W m^{-2} and the maximum underestimation is -10.1 W m^{-2}. Both the simulated and observed H are negative during the night (1700–0700 UTC). The simulation and observation of H are 1 h out of phase in their diurnal cycle. The errors in the estimation of H are primarily related to the errors in the estimation of both Q and G_0, the ground heat flux (to be discussed later). To prove this assertion, two curves of the observed and simulated total

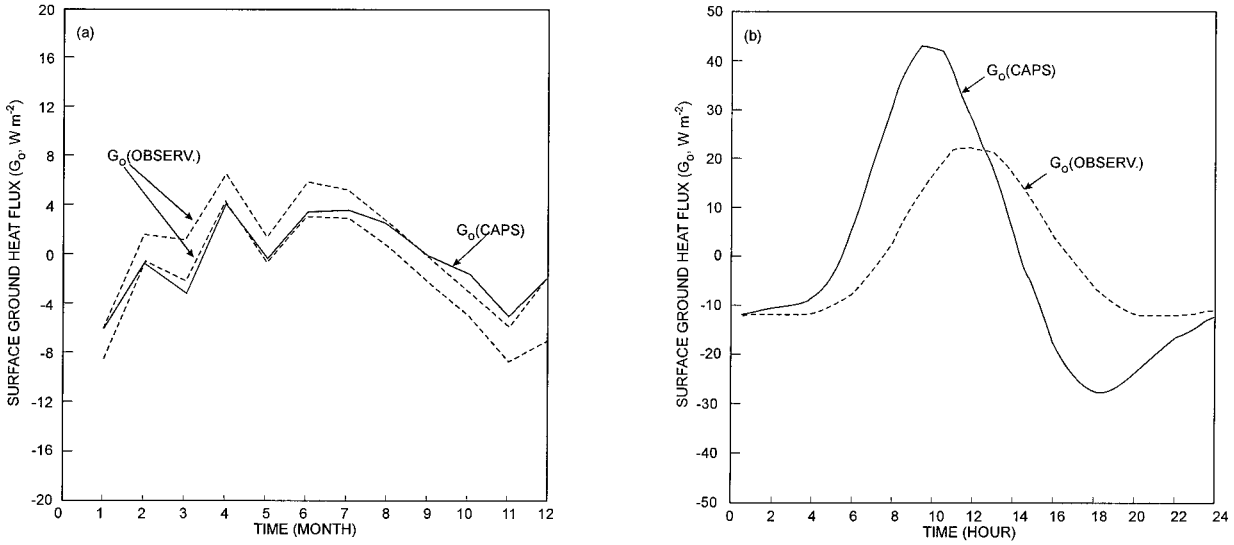

FIG. 7. (a) Seasonal and (b) diurnal (averaged over 1 yr) variations of simulated (solid line) and observed (dashed line) surface ground heat flux (G_0). The two dashed lines in (a) indicate the upper- and lower-error bonds of the observed G_0.

heat fluxes (H + LE + G_0) are plotted in the upper part of Fig. 6b. These two curves appear close to each other without a phase difference. However, the simulated total heat flux still appears too small during the night. As shown by Fig. 2, the Richardson number is positive (Ri $>$ 0) during the night. If the bulk exchange coefficient for heat (C_h) were smaller for Ri $>$ 0, then the scheme would have predicted a smaller downward (negative) sensible heat flux. Then, it could have reduced the underestimation of H during the night. This implies that the stability correction function F_h for Ri $>$ 0 in (9), which is the same as F_m in (8), could have been overestimated as discussed before.

6) SURFACE GROUND HEAT FLUX (G_0)

Figure 7 shows the seasonal and diurnal variations for surface ground heat flux (G_0). As before, the two dashed lines in Fig. 7a are the upper- and lower-error bounds around the observed G_0. In fact, G_0 at Cabauw was not directly measured. It was inferred by either a λ method or a Fourier method (BB97). The simulated G_0 was computed by (11b) or (20a). Figure 7a shows that the seasonal variation of the monthly average of G_0 is approximately in the range from -7 to 5 W m^{-2}. The CAPS scheme appears to overestimate G_0 from August to January, while underestimating it from February to July.

Figure 7b shows that there are significant differences in both amplitude and phase in the diurnal cycle of G_0 between the simulation and observation. The simulated amplitude is about 43.0 W m^{-2}, while the observed amplitude is about 22.6 W m^{-2}. The phase difference is 2.5 h. These discrepancies can hardly be attributed to a single factor in the CAPS scheme. They are more likely related to two aspects. First is the difference between the real soil structure and that specified in the scheme. As described by BB97, there are actually five distinct soil layers with different depths and soil textures at Cabauw. The current standard version of the scheme has only two soil layers (Fig. 1) and one soil type. Second is the lack of vegetation effects on the ground heat flux. As pointed out by Xinmei and Lyons (1995), the formulation of (11b), which does not take vegetation into account, could overestimate G_o over vegetated land.

5. Conclusions

We have presented a comprehensive description of the most updated version of the CAPS land surface parameterization scheme. This scheme is the land surface scheme in the Oregon State University and Phillips Laboratory atmospheric boundary layer and plant–soil model for application to large-scale numerical weather prediction or general circulation models. The CAPS scheme, in our view, includes most essential physics and has a relatively simple and robust algorithm.

From an historical point of view, several major features have provided the framework for successful applications. The first feature is the replacement of the usual force–restore equations with the actual equations for heat and moisture transport in the soil. These equations allow application of the expertise and observations of the soil physics community. The second feature is the air-dry value (Θ_{dry}) approach for the parameterization of soil evaporation. The concept and implementation in computation of the skin temperature (T_{sfc}) play a key role for simultaneous evaluation of sensible and surface ground heat fluxes. The use of an effective depth, (21), for soil heat flux calculation under the snow

cover situation allows for a smooth transition as snow cover reduces to zero thickness. Another feature is the inclusion of precipitation-related heat fluxes in (11a).

Our participation in PILPS has allowed the CAPS scheme to be tested in a zero-dimensional mode, which is a single-point model simulation of land surface and soil processes driven by prescribed atmospheric forcing (i.e., the 1987 Cabauw) dataset. This zero-dimensional (stand-alone) approach is a good experimental design since it can avoid complicated coupling effects and help relate model performance with model physics more easily than in one-, two-, or three-dimensional experiments. In PILPS phase 1, simulations have been made for tropical rain forest and grassland regions representing a typical scale of a GCM gridbox. Generally, the CAPS scheme performed adequately with realistic surface energy and water balances (Pitman et al. 1993). However, there were no observational validation data in PILPS phase 1. Fortunately, in phase 2 of PILPS, an observational dataset from the Cabauw field site in the Netherlands was provided to test CAPS and other schemes. This Cabauw dataset is very valuable and unique because it includes an entire year of both forcing data and validation data (surface fluxes). As shown in the last section, the results from the CAPS experimentation show that, for long-term integration (monthly and yearly averages), the CAPS scheme performs well when compared to Cabauw (1987) validation data.

The results of our numerical experiment, on the other hand, also indicate several opportunities for improvement to the CAPS scheme. The standard version of the scheme has two soil layers with fixed depths and does not allow water table movement that can be important during long drying periods; this has been modified in a newer version of the CAPS scheme. Also, the treatment of the canopy in the CAPS scheme ignores canopy dynamics, which can be important in some circumstances. In the presence of vegetation, soil heat flux is lessened due to lower heat conductivity through overlying vegetation, while a parameterization to account for this effect is not part of the standard CAPS scheme. The approach described in Viterbo and Beljaars (1995) has been incorporated into a version of the CAPS scheme and has performed favorably. The snow subscheme needs further improvement, for example, fractional snow coverage is currently not accounted for, and there is no consideration made for the soil–ice phase. The albedo and roughness length are prescribed in the CAPS scheme rather than parameterized in terms of vegetation, soil moisture, time of day, snow cover, etc. The formulation of the bulk transfer coefficients (C_m, C_h), especially for stable stratification, needs further examination [e.g., the Louis-type explicit bulk Richardson number approach by Van den Hurk and Holtslag (1997)]. This topic is closely related to the effect of subgrid variability, which has important consequences for estimation of area-averaged surface fluxes. Sun and Mahrt (1995), for example, have shown that the use of surface radiative temperature computed from a surface energy balance can induce significant errors in the parameterization of surface fluxes, especially sensible heat flux.

Finally, testing to date has not included a persistent snow cover and cold season processes, for example, PILPS phase 2(d), Valdai (Russia) experiment (see Schlosser et al. 1997). The recent PILPS phase 2(c) was designed to focus on important hydrological aspects for the Arkansas–Red River Basin (Abdulla et al. 1995). The participation of the CAPS scheme in PILPS 2(c) has allowed further testing of the scheme and hence provide more opportunities for improvement, as suggested above, for example, more soil layers, subroot zone, etc.

Acknowledgments. Professor Larry Mahrt, Oregon State University, who was one of the original designers of the OSU/PL model, contributed many valuable inputs and comments. We acknowledge the Royal Netherlands Meteorological Institute (KNMI) for providing the Cabauw data, which are the result of a long-term boundary layer monitoring program in the Netherlands. Dr. A. Beljaars (currently at the European Centre for Medium-Range Weather Forecasts) and Dr. F. Bosveld at KNMI have made many valuable suggestions for our use of the Cabauw data (release 3). With over 12 years of development with the CAPS scheme, many people need to be acknowledged for their contribution and help in developing this model. This has been done primarily in four internal technical reports. Recently, we have had many exchanges of experiences and comments on the CAPS scheme with Dr. K. Mitchell, Dr. F. Chen, both at the National Centers for Environmental Prediction, Environmental Modeling Center, NOAA; Prof. R. Cuenca at the Department of Bioresource Engineering, Oregon State University; and Dr. Jimwon Kim, at Lawrence Livermore National Laboratory, University of California. Our thanks go to Mr. Donald Chisholm, chief of the Tactical Environmental Support Branch of the Air Force Research Laboratory, for his constant support and encouragement. The comments of the three anonymous reviewers are much appreciated. Ms. Audrey Campana, at the Battlespace Environment Division, Air Force Research Laboratory, has typed many versions of the manuscript with great patience and excellent skill.

REFERENCES

Abdulla, F. A., D. P. Lettenmaier, E. F. Wood, and J. A. Smith, 1995: Comparison of evaporation for the Red-Arkansas Basin. *GEWEX News,* **5** (4), 1–7.

Al Nakshabandi, G., and H. Kohnke, 1965: Thermal conductivity and diffusivity of soils as related to moisture tension and other physical properties. *Agric. Meteor.,* **2,** 271–279.

Beljaars, A. C. M., 1995: Precipitation observations at Cabauw. KNMI Memo. A0-95-08, 34 pp. [Available from KNMI, P.O. Box 201, 3730 AE, De Bilt, the Netherlands.]

——, and P. Viterbo, 1994: The sensitivity of winter evaporation to the formulation of aerodynamic resistance in the ECMWF model. *Bound.-Layer Meteor.,* **71,** 135–149.

——, and F. C. Bosveld, 1997: Cabauw data for the validation of land surface parameterization schemes. *J. Climate,* **10,** 1172–1193.

Brutsaert, W. H., 1982: *Evaporation into the Atmosphere*. D. Reidel, 299 pp.

Chang, S., and M. Ek, 1996: Sensitivity study of the CAPS Model land-surface scheme using the 1987 Cabauw/PILPS dataset. *Phys. Chem. Earth,* **21,** 205–210.

Chen, F., and Coauthors, 1996: Modeling of land-surface evaporation by four schemes and comparison with FIFE observations. *J. Geophys. Res.,* **101,** 7251–7268.

Chen, T. H., and Coauthors, 1997: Cabauw experimental results from the Project for Intercomparison of Land-Surface Parameterization Schemes. *J. Climate,* **10,** 1194–1215.

Clapp, R. B., and G. M. Hornberger, 1978: Empirical equations for some soil hydraulic properties. *Water Resour. Res.,* **14,** 601–604.

Cosby, B. J., G. M. Hornberger, R. B. Clapp, and T. R. Ginn, 1984: A statistical exploration of the relationship of soil moisture characteristics of the physical properties of soils. *Water Resour. Res.,* **20,** 682–690.

Deardorf, J. W., 1978: Efficient prediction of ground surface temperature and moisture, with inclusion of a layer of vegetation. *J. Geophys. Res.,* **83** (C4), 1889–1903.

Dickinson, R. E., A. Henderson-Sellers, and P. J. Kennedy, 1993: Biosphere–Atmosphere Transfer Scheme (BATS) version as coupled to the NCAR community climate model. NCAR Tech. Note NCAR/TN-387+STR, National Center for Atmospheric Research, Boulder, CO, 72 pp. [Available from Publication Office, NCAR, P.O. Box 3000, Boulder, CO 80307.]

Ek, M., and L. Mahrt, 1991a: A model for boundary-layer cloud cover. *Ann. Geophys.,* **9,** 716–724.

——, and ——, 1991b: OSU 1-D Model user's guide (version 1.0.4). Oregon State University, Corvallis, OR, 216 pp.

——, and R. H. Cuenca, 1994: Variations in soil parameters: Implication for modeling surface fluxes and atmospheric boundary layer development. *Bound.-Layer Meteor.,* **70,** 369–383.

Feddes, R. A., E. Bresier, and S. P. Neuman, 1974: Field test of a modified numerical model for water uptake by root systems. *Water Resour. Res.,* **10,** 1199–1206.

Garratt, J. R., 1992: *The Atmospheric Boundary Layer*. Cambridge University Press, 316 pp.

Gray, D. M., and D. H. Male, 1981: *Handbook of Snow*. Pergamon Press, 776 pp.

Hanks, R. J., A. Klute, and E. Bresier, 1969: A numeric method for estimating infiltration redistribution, drainage, and evaporation of water from soil. *Water Resour. Res.,* **5,** 1063–1069.

Henderson-Sellers, A., Z.-L. Yang, R. E. Dickinson, P. J. Kennedy, and K. McGuffie, 1993: The Project for Intercomparison of Land Surface Parameterization Schemes. *Bull. Amer. Meteor. Soc.,* **74,** 1335–1349.

——, A. J. Pitman, P. K. Love, P. Irannejad, and T. H. Chen, 1995: The Project for Intercomparison of Land Surface Parameterization Schemes (PILPS): Phases 2 and 3. *Bull. Amer. Meteor. Soc.,* **76,** 489–503.

Hillel, D., 1982: *Introduction to Soil Physics*. Academic Press, 364 pp.

Jacobs, C. M. J., and H. A. R. De Bruin, 1992: The sensitivity of regional transpiration to land-surface characteristics: Significance of feedback. *J. Climate,* **5,** 683–698.

Jacquemin, B., and J. Noilhan, 1990: Sensitivity study and validation of a land surface parameterization using the HAPEX MOBILHY dataset. *Bound.-Layer Meteor.,* **52,** 93–134.

Jarvis, P. G., 1976: The interpretation of the variations of leaf water potential and stomatal conductance found in canopies in the field. *Philos. Trans. Roy. Soc. London,* **273B,** 593–610.

Kim, J., and M. Ek, 1995: A simulation of the surface energy budget and soil water content over the HAPEX-MOBILHY forest site. *J. Geophys. Res.,* **100,** 20 845–20 854.

Kondo, J., H. Saigusa, and T. Sato, 1990: A parameterization of evaporation from bare soil surfaces. *J. Appl. Meteor.,* **29,** 385–389.

Lee, T. J., and R. A. Pielke, 1992: Estimating the soil surface specific humidity. *J. Appl. Meteor.,* **31,** 480–484.

Louis, J. F., M. Tiedke, and J. F. Geleyn, 1982: A short history of the operational PBL-parameterization at ECMWF. *Workshop on Planetary Boundary Layer Parameterization,* European Centre for Medium-Range Weather Forecasts, 59–79.

Mahrt, L., 1987: Grid-averaged surface fluxes. *Mon. Wea. Rev.,* **115,** 1550–1560.

——, and M. Ek, 1984: The influence of atmospheric stability on potential evaporation. *J. Climate Appl. Meteor.,* **23,** 222–234.

——, and H.-L. Pan, 1984: A two-layer model of soil hydrology. *Bound.-Layer Meteor.,* **29,** 1–20.

McCumber, M. C., and R. A. Pielke, 1981: Simulation of the effects of surface fluxes of heat and moisture in a mesoscale numerical model. 1. Soil layer. *J. Geophys. Res.,* **86** (C10), 9929–9938.

Nimah, M. N., and R. J. Hanks, 1973: Model for estimating soil water, plant, and atmospheric interrelations: I. Description and sensitivity. *Soil Sci. Soc. Amer. Proc.,* **37,** 522–527.

Noilhan, J., and S. Planton, 1989: A simple parameterization of land surface processes for meteorological models. *Mon. Wea. Rev.,* **117,** 536–549.

Norquist, D., and S. Chang, 1994: Diagnosis and corrections of systematic humidity errors in a global numerical weather prediction model. *Mon. Wea. Rev.,* **122,** 2442–2460.

Pan, H.-L., 1990: A simple parameterization scheme of evapotranspiration over land for the NMC medium-range forecast model. *Mon. Wea. Rev.,* **118,** 2500–2512.

——, and L. Mahrt, 1987: Interaction between soil hydrology and boundary-layer development. *Bound.-Layer Meteor.,* **38,** 185–202.

Phillip, J. R., 1957: Evaporation, and moisture and heat fields in the soil. *J. Meteor.,* **14,** 354–366.

Pielke, R. A., 1984: *Mesoscale Meteorological Modeling*. Academic Press, 612 pp.

Pitman, A. J., and Coauthors, 1993: Project for Intercomparison of Land-Surface Parameterizations Schemes (PILPS): Results from off-line control simulations (phase 1a). International GEWEX Project Office Publication Series 7, World Climate Research Programme, 47 pp.

Schlosser, C. A., A. J. Pitman, A. G. Slater, and A. Henderson-Sellers, 1997: Experimental design and preliminary results from PILPS Phase 2(d). *GWEX News,* **7** (4), 9–11.

Sellers, P. J., Y. Mintz, Y. C. Sud, and A. Dalcher, 1986: A simple biosphere model (SiB) for use within general circulation models. *J. Atmos. Sci.,* **43,** 505–531.

Sun, J., and L. Mahrt, 1995: Determination of surface fluxes from the surface radiative temperature. *J. Atmos. Sci.,* **52,** 1096–1106.

Troen, I., and L. Mahrt, 1986: A simple model of the atmospheric boundary layer: Sensitivity to surface evaporation. *Bound.-Layer Meteor.,* **37,** 129–148.

Van den Hurk, B. J. J. M., and A. A. M. Holtslag, 1997: On the bulk parameterization of surface fluxes for various conditions and parameter ranges. *Bound.-Layer Meteor.,* **82,** 119–134.

Viterbo, P., and A. C. M. Beljaars, 1995: An improved land surface parameterization scheme in the ECMWF model and its validation. *J. Climate,* **8,** 2716–2748.

Wetzel, P. J., and J.-T. Chang, 1987: Concerning the relationship between evapotranspiration and soil moisture. *J. Climate Appl. Meteor.,* **26,** 18–27.

Wilson, M. F., A. Henderson-Sellers, R. E. Dickinson, and P. J. Kennedy, 1987: Investigation of the sensitivity of the land-surface parameterization of the NCAR community climate model in regions of tundra vegetation. *J. Climatol.,* **7,** 319–343.

Xinmei, H., and T. J. Lyons, 1995: The simulation of surface heat fluxes in a land surface–atmosphere model. *J. Appl. Meteor.,* **34,** 1099–1111.

Yang, Z.-L., R. E. Dickinson, A. Robock, and K. Ya. Vinnikov, 1997: Validation of the snow submodel of the Biosphere–Atmosphere Transfer Scheme with Russian snow cover and meteorological observational data. *J. Climate,* **10,** 353–373.

Zinke, P. J., 1967: Forest interception studies in the United States. *Forest Hydrology,* W. E. Sopper and H. W. Lull, Eds., Pergamon, 137–161.